THE ASTROPHYSICAL JOURNAL, 507:968–973, 1998 November 10

FORMATION OF CURRENT SHEETS IN TWO-DIMENSIONAL GEOMETRY

R. A. SCHEPER[1] AND A. B. HASSAM
Institute for Plasma Research, University of Maryland, College Park, MD 20742
Received 1998 March 11; accepted 1998 June 12

ABSTRACT

We present two examples of current sheets that form in a magnetic configuration when it is subjected to quasi-static motions at the footpoints. The entire system is two-dimensional. There are no preexisting X-points and the footpoint motions are continuous. The calculations are motivated by the hypothesis of Parker that quasi-static deformations of MHD equilibria are generally accompanied by the formation of current sheets. The results demonstrate that three dimensions are not a necessary condition for current sheet formation. In addition, the calculation of Van Ballegooijen is not contradicted, because the initial magnetic field in our case is not dominantly collinear. Possible applications to the solar corona are discussed.

Subject headings: MHD — Sun: corona — Sun: magnetic fields

1. INTRODUCTION

The outer layers of the Sun are magnetized plasmas consisting of the dense convection zone, the photosphere, and the tenuous corona. The corona is a hot, low-β, highly ideal MHD plasma, with density stratified by the solar gravitational field. Immediately below the corona exists the photosphere, the interface marked by the depth below which the plasma becomes dense enough to be opaque to visible light. Threaded throughout the corona-photosphere region are magnetic fields. Since the plasma is well described by MHD and the Reynolds numbers are very large, the magnetic fields are "frozen-in," i.e., they are convected along with the plasma mass. These fields typically form localized looplike structures in the corona, with their "ends" dipping back into the photosphere and presumably entering the solar convection zone. Since the subphotospheric region is much more dense than the corona, its motion is thought to be the driving force behind magnetic deformations in the corona. In addition, the interface between the photosphere and the corona has a much sharper spatial scale than these loop structures in general, owing to the short gravitational scale height. Thus the photosphere is an effective "boundary" at which the field is "line-tied." Regions where the loops intersect this boundary can be thought of as "footpoints." The footpoint motions determine the magnetic changes in the corona.

One of the outstanding questions in solar physics is whether or not the slow, churning photospheric deformations can cause spontaneous discontinuities in the coronal magnetic field. If this is indeed the case, then this may shed some light on the coronal heating problem (Zirker 1993), since such discontinuities could generate currents large enough to significantly heat the corona. Parker (1994) has proposed that slow, sub-Alfvénic deformations of a three-dimensional equilibrium lead generally to "loss of equilibrium" resulting in current sheet discontinuities. On the other hand, in a calculation wherein the cross-field displacements are small compared with the scale length along the field, Van Ballegooijen (1985) found no appearance of such current sheets; nonsingular neighboring equilibria were always found. The only exceptions, according to the latter and other calculations, are if the driving deformations are themselves discontinuous or if the initial configuration harbors a null in the magnetic field (Syrovatskii 1971; Antiochos 1987; Hassam & Lambert 1996). In particular, Van Ballegooijen assumes a uniform collinear magnetic field connecting the footpoints about which deformations are forced.

Generally speaking, it has proved difficult to find simple, test-case examples to prove or disprove the above two seemingly conflicting scenarios. To be sure, many interesting test cases that generate current sheets have been examined (Low 1987, 1989, 1991; Low & Wolfson 1988; Vekstein, Priest, & Amari 1991). In all these calculations, there were no nulls in the initial equilibrium and the footpoint motions were not discontinuous. In this sense, our present calculations have much in common with these earlier papers, and the physical reasons why current sheets were obtained in both sets of calculations are also quite similar. However, the calculations we present in this paper can be characterized as being relatively simple from an analytical standpoint: in the two cases we present, a complete and unequivocal solution is possible with a minimum of algebra. For the purposes of this paper, it is pedagogically advantageous to first present our two cases and then discuss the above-mentioned previous work in the context of our results. A comparison with previous work is given in the discussion section.

As mentioned, we were motivated to demonstrate current sheet formation (or failure thereof) by considering the simplest possible geometries that would allow this. Such a demonstration would have to be for continuous footpoint motions, and no magnetic nulls were to be allowed in the initial configuration. Indeed, we present in this paper two simple examples of current sheet formation. The calculations are almost completely analytically tractable, and an unequivocal conclusion is possible. In demonstrating current sheet formation, we are in support of Parker's scenario. However, our results do not contradict Van Ballegooijen's calculation. The reason for this is that Van Ballegooijen's initial magnetic field lines run from one footpoint and all end up at another footpoint; in our examples, we relax this assumption. Our initial magnetic field lines start from one footpoint, but some of these flux lines end up at one footpoint and some end up at another, uncorrelated, footpoint. Thus Van Ballegooijen's proof does not apply to our examples. As will become clear below, our chosen initial

[1] scheper@glue.umd.edu.

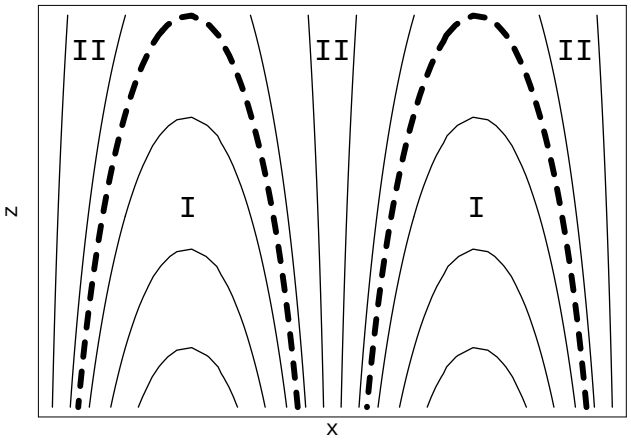

FIG. 1.—Initial field $\psi = (B_0/k)e^{-kz}\sin(kx)$ in the domain $-\pi < kx < \pi$, $0 < z < L$. The dashed lines denote the critical field lines $|\psi| = (B_0/k)e^{-kL}$, which separate regions I and II.

configuration is smooth and continuous even though field lines end up at different footpoints. To reiterate, our model incorporates several features that address the concerns discussed above. First, the initial magnetic field contains no discontinuities, and the scale of spatial variation is comparable to the system size. Second, the initial field contains no nulls. Third, the boundary (footpoint) displacements are continuous and smooth on the spatial scale of the system; in fact, they are relatively simple displacements. Finally, the footpoint motions are slow, i.e., much slower than the Alfvén speed. This renders the model quasi-static and is consistent with solar coronal parameters.

We begin by describing our model in the next section. In § 3 we present an analytic solution for current sheets that arise from axial footpoint motions. In § 4 we present another example of current sheet formation involving the same initial field, but with transverse footpoint motions. This case requires a partial numerical treatment. Finally, in § 5 we discuss previous work done by others and possible implications for the solar corona.

2. MODEL

A quasi-static, low-β, ideal MHD plasma is governed by the following equations (Gaussian units):

$$\boldsymbol{J} = \frac{c}{4\pi}\nabla \times \boldsymbol{B}\,, \tag{1}$$

$$\boldsymbol{J} \times \boldsymbol{B} = 0\,, \tag{2}$$

$$\frac{\partial \boldsymbol{B}}{\partial t} = -c\nabla \times \boldsymbol{E}\,, \tag{3}$$

$$\boldsymbol{E} = -\frac{\boldsymbol{u} \times \boldsymbol{B}}{c}\,, \tag{4}$$

$$\nabla \cdot \boldsymbol{B} = 0 \tag{5}$$

where $\boldsymbol{B}$ is the magnetic field, $\boldsymbol{E}$ is the electric field, $\boldsymbol{u}$ is the mass flow, $\boldsymbol{J}$ is the current, and c is the speed of light.

Consider a system with two parallel conducting plates at $z = 0$ and $z = \mathrm{L}$, which are infinite in extent in the $\hat{x}$ and $\hat{y}$ directions. Between these plates exists an ideal MHD plasma. Here, the plates play the role of the photosphere-corona interface, while the plasma can be thought of as the corona. We restrict ourselves to a two-dimensional system, i.e., we impose $\partial_y = 0$. Threaded through this system is an equilibrium magnetic field $\boldsymbol{B}(\boldsymbol{x}_\perp)$, where $\boldsymbol{x}_\perp = x\hat{x} + z\hat{z}$. Since $\partial_y = 0$, and from equation (5), $\boldsymbol{B}$ can be written, in general, as

$$\boldsymbol{B}(\boldsymbol{x}_\perp) = B_y\hat{y} + \hat{y} \times \nabla_\perp \psi(\boldsymbol{x}_\perp)\,, \tag{6}$$

where $\nabla_\perp = \hat{x}\partial_x + \hat{z}\partial_z$. Using equation (6), we cast equations (1)–(5) in a more convenient form (Hassam & Lambert 1996):

$$\nabla_\perp \frac{B_y^2}{2} + \nabla_\perp \psi \nabla_\perp^2 \psi = 0\,, \tag{7}$$

$$\boldsymbol{B}_\perp \cdot \nabla_\perp B_y = 0\,, \tag{8}$$

$$\frac{\partial \psi}{\partial t} = -\boldsymbol{u}_\perp \cdot \nabla_\perp \psi\,, \tag{9}$$

$$\frac{\partial B_y}{\partial t} = -\boldsymbol{u}_\perp \cdot \nabla_\perp B_y - B_y \nabla_\perp \cdot \boldsymbol{u}_\perp + \boldsymbol{B}_\perp \cdot \nabla_\perp u_y\,. \tag{10}$$

As a general initial condition for both cases treated in this paper, we choose for the magnetic field

$$B_y(t = 0) = 0\,, \tag{11}$$

$$\psi(t = 0) = \frac{B_0}{k}\,e^{-kz}\sin(kx)\,, \tag{12}$$

where the wavenumber k is an arbitrary real constant. In general, we consider k to be of order L^{-1}. See Figure 1 for a sketch of this system. Notice that in addition to the properties mentioned above, this field possesses other important features. Chief among these is that the structure of $\boldsymbol{B}$ allows for the distinction between two fundamentally different kinds of regions in the plasma. Region I field lines intersect the bottom plate ($z = 0$) only, while region II field lines intersect both the bottom and top plates. The critical field lines that separate the two regions just graze the top plate. Note that the system is periodic in the $\hat{x}$-direction.

In what follows, we consider two cases. For case 1, the top plate ($z = L$) is pulled rigidly in the $\hat{y}$-direction, while the bottom plate is held fixed. As will be shown, this gives rise to immediate discontinuities in the magnetic field. For case 2, the top plate is pulled rigidly in the $\hat{x}$-direction while the bottom plate is held fixed. As will be shown, this does not give rise to immediate current sheets; rather, they appear spontaneously after a critical displacement ξ_c. Note that in both cases there are no nulls or discontinuities at $t = 0$. We describe each of these cases in turn in the following sections.

3. CASE 1: AXIAL DISPLACEMENTS

Let the equilibrium field given by equations (6)–(8) exist at time $t = 0$. We now set the top plate in motion with a rigid displacement whose velocity is

$$|\boldsymbol{u}|_{z=L} = \dot{\xi}(t)\hat{y}\,, \tag{13}$$

where the displacement $\xi(t)$ is an arbitrary function of time and the dot denotes differentiation with respect to t. We let the bottom plate remain fixed, i.e.,

$$|\boldsymbol{u}|_{z=0} = 0\,. \tag{14}$$

The boundary conditions at the plates must be consistent with the fact that they are perfect solid conductors. Thus we have the familiar constraints that $\boldsymbol{E} \cdot \hat{\boldsymbol{t}}$ and $\boldsymbol{B} \cdot \hat{\boldsymbol{n}}$ must be

continuous at those interfaces. This implies that $\boldsymbol{u} \cdot \hat{\boldsymbol{t}}$ is also continuous at the plates, and so we have all the information we need to solve the problem. We assume that $\ddot{\xi}(t)$ is sufficiently small to maintain a force-free system.

Let us consider small perturbations, i.e., assume $|\xi(t)| \ll L$. Since the coronal plasma is ideal, the frozen-in theorem is applicable, and we expect that the magnetic perturbation at any point is proportional to the displacement at that point. Therefore, small displacements also imply that the ordering $B_y \ll |\boldsymbol{B}_\perp|$ is appropriate. In this limit, B_y, u_y decouple from the remaining variables, as can be readily checked from equations (7)–(10). Since the only nonzero boundary condition is on u_y, we are free to set those remaining variables to zero and need not consider them further.

At this point, it is convenient to introduce the field coordinate Λ, defined by

$$\nabla_\perp \Lambda \equiv \hat{\boldsymbol{y}} \times \nabla_\perp \psi = \boldsymbol{B}_\perp , \tag{15}$$

namely

$$\Lambda = \frac{B_0}{k} e^{-kz} \cos (kx) . \tag{16}$$

It will be more convenient to work in the new orthogonal coordinates ψ, Λ. Note that field lines can be defined as curves of constant ψ, and the background magnetic field $\boldsymbol{B}_\perp$ is strictly in the $\nabla_\perp \Lambda$ direction. Using the new coordinates, equation (8) becomes

$$\frac{\partial B_y}{\partial \Lambda} = 0 . \tag{17}$$

Thus B_y is strictly a function of ψ and t. Equation (10) becomes

$$\frac{\partial B_y}{\partial t} = B_\perp^2 \frac{\partial u_y}{\partial \Lambda} . \tag{18}$$

By making use of equation (17), we can immediately integrate equation (18) along an entire field line in the corona to get

$$(u_y)_{\text{endpoints}} = \frac{\partial B_y}{\partial t} \oint \frac{d\Lambda}{B_\perp^2} . \tag{19}$$

The integral is taken over a field line starting from the bottom plate and culminating either at the top or the bottom plate depending on the field line (see Fig. 1). Since $(u_y)_{\text{endpoints}}$ is known, the remaining freedom is fixed and the solution for B_y is obtained.

The importance of the differences between regions I and II becomes apparent when considering the possible paths of integration in equation (19). In region I all fields end at the bottom plate without ever reaching the top plate. Thus we choose the final point of integration Λ_f at $z = 0$. In that case, the left-hand side of equation (19) vanishes. This immediately implies

$$B_y(\psi, t) = 0 , \quad |\psi| > \frac{B_0}{k} e^{-kL} . \tag{20}$$

In contrast, all region II field lines reach the top plate, and so we choose Λ_f at $z = L$ to make use of boundary condition (13). Solving for B_y in equation (19) gives

$$B_y(\psi, t) = \xi(t) k^2 \psi \left[\arcsin \left(\frac{k\psi}{B_0} \right) - \arcsin \left(\frac{k\psi e^{-kL}}{B_0} \right) \right]^{-1} ,$$

$$|\psi| < \frac{B_0}{k} e^{-kL} . \tag{21}$$

It is clear that B_y is discontinuous at the critical value $|\psi_{\text{crit}}| = (B_0/k)e^{-kL}$, and thus current sheets indeed exist for $t > 0$ at $\psi = \psi_{\text{crit}}$ (see Fig. 1).

The physics of this situation is straightforward. As the top plate moves forward along $\hat{\boldsymbol{y}}$, it drags the field in the plate with it via the frozen-in theorem. The field at the bottom plate, however, is anchored in place. Thus the field lines must "tip" in the $\hat{\boldsymbol{y}}$ direction, which is why B_y must be generated. Since the plasma is ideal and the field is being "sheared" into a symmetry direction, the tip of each individual field line is independent of neighboring field lines, i.e., field lines exert no drag forces on one another. Thus the tip of each field line is governed by how it intersects the top plate. The field lines that never reach the top plate have nothing to pull on them, so B_y is never generated. However, any field line that does intersect the plate must be pulled along no matter how shallow the angle of intersection, thus generating a nonzero B_y. Therefore, current sheets must develop between the field lines that tip and those that do not.

4. CASE 2: TRANSVERSE DISPLACEMENTS

For this case, instead of the symmetry direction $\hat{\boldsymbol{y}}$, we let the top plate move rigidly in the $\hat{\boldsymbol{x}}$-direction with velocity

$$|\boldsymbol{u}|_{z=L} = \dot{\xi}(t)\hat{\boldsymbol{x}} , \tag{22}$$

and let the bottom plate be held fixed as in case 1. This case is more difficult and requires some numerical treatment for a full solution. Nonetheless, we can establish the appearance of current sheets from analytical considerations.

Let us consider the boundary conditions for this case. The initial magnetic field is given by equations (6), and (12). Specifically, we have

$$\boldsymbol{B}_\perp = -B_0 e^{-kz} [\cos (kx)\hat{\boldsymbol{z}} + \sin (kx)\hat{\boldsymbol{x}}] , \tag{23}$$

which is the field at $t = 0$, or equivalently $\xi(t = 0) = 0$. As stated previously, equations (3) and (5) imply that the tangential electric field and normal magnetic field must be continuous at the plates. For the bottom plate, this implies

$$B_z|_{z=0} = -B_0 \cos (kx) , \quad |\boldsymbol{E} \cdot \hat{\boldsymbol{t}}|_{z=0} = 0 , \quad |\boldsymbol{u} \cdot \hat{\boldsymbol{t}}|_{z=0} = 0 . \tag{24}$$

To recover the boundary conditions for the top plate, we make use of the frozen-in theorem. Since the top plate is a perfect conductor, the magnetic field in that plate must be convected along at the velocity given by equation (22). Since the plate is rigid ($\boldsymbol{u}|_{z=L}$ has no spatial variation), we can infer the magnetic field in the plate in the lab frame by using the simple Galilean transformation $x \to x - \xi(t)$. Thus the boundary condition for the magnetic field at the top plate becomes

$$B_z|_{z=L} = -B_0 e^{-kL} \cos [kx - k\xi(t)] . \tag{25}$$

The electric field boundary condition, given by equations (3) and (22), is

$$|\boldsymbol{E}\cdot\hat{\boldsymbol{t}}|_{z=L} = -\frac{B_0\,\dot{\xi}}{c}\,e^{-kL}\cos\,[kx - k\xi(t)]\hat{y}\,. \quad (26)$$

This system can be simplified in a manner similar to case 1. Note that the above boundary conditions do not force any contribution from B_y or u_y. In that case, it can be seen from equations (7)–(10) that B_y and u_y can be set to zero. This leaves

$$\nabla_\perp\psi\nabla_\perp^2\psi = 0\,, \quad (27)$$

$$\frac{\partial\psi}{\partial t} = -\boldsymbol{u}_\perp\cdot\nabla_\perp\psi\,, \quad (28)$$

as the remaining equations to solve. Note that no linearization has been done in obtaining these equations.

We proceed as follows. The initial magnetic field is nonzero everywhere in the domain. As long as this remains the case during the displacement, $\nabla_\perp\psi \neq 0$ and thus from equation (27),

$$\nabla_\perp^2\psi(\boldsymbol{x}_\perp, t) = 0\,. \quad (29)$$

Now, a unique solution to equation (29) exists if we know the boundary conditions. The initial condition is given by equation (12):

$$\psi|_{t=0} = \frac{B_0}{k}\,e^{-kz}\sin\,(kx)\,. \quad (30)$$

To obtain an equation for $\boldsymbol{E}$, we substitute for $\boldsymbol{B}_\perp$ in Faraday's law (eq. [3]) using equation (6). The resulting equation can be inverted to give

$$\boldsymbol{E} = \frac{\dot{\psi}}{c}\,\hat{y}\,. \quad (31)$$

From this and equations (24)–(26) we generate the necessary boundary conditions on ψ:

$$\psi|_{z=0} = \frac{B_0}{k}\sin\,(kx)\,, \quad \psi|_{z=L} = \frac{B_0}{k}\,e^{-kL}\sin\,[kx - k\xi(t)]\,. \quad (32)$$

Thus the unique solution to equation (29) with the boundary condition in equation (32) is given by

$$\psi = \frac{B_0}{k}\,e^{-kL}\frac{\sinh\,(kz)}{\sinh\,(kL)}\sin\,[kx - k\xi(t)] + \frac{B_0}{k}\frac{\sinh\,(kL - kz)}{\sinh\,(kL)}\sin\,(kx)\,. \quad (33)$$

Equation (31) gives, for the electric field,

$$\boldsymbol{E} = -\frac{B_0\,\dot{\xi}}{c}\,e^{-kL}\frac{\sinh\,(kz)}{\sinh\,(kL)}\cos\,[kx - k\xi(t)]\,. \quad (34)$$

Thus we have found unique solutions for $\boldsymbol{B}_\perp$ and $\boldsymbol{E}$ that are well behaved everywhere.

However, a problem arises when we consider u_ψ. This cross-field flow can be calculated directly from equations (4) and (31):

$$u_\psi = -\frac{\dot{\psi}}{|\nabla_\perp\psi|} = \frac{\boldsymbol{u}\cdot\nabla_\perp\psi}{|\nabla_\perp\psi|}\,. \quad (35)$$

Evidently, if $|\nabla_\perp\psi|$ vanishes for nonzero $\dot{\psi}$, then u_ψ diverges and the solution must be discarded. Thus equation (29) is not correct at the point in time where $\nabla_\perp\psi = 0$. Now, as we pointed out, there were no nulls in the equilibrium we started out with. Subsequently, as we displace the top plate, the solution given by equation (33) can be examined for nulls that might develop. We find that indeed there are nulls in equation (33) for $t > 0$, but, for early times, these nulls are outside the domain of the problem, i.e., for $z > L$. We emphasize that for these early times, the nulls outside the domain are physically irrelevant, since we have a solution inside the domain that satisfies the boundary conditions. Having said this, it is nonetheless mathematically instructive to examine these outside nulls as time progresses, as we discuss below.

The possibility remains that the solution (eq. [33]) could eventually admit a null that appears inside the domain $0 < z < L$. In such an event, at and beyond this critical time another solution must be found—any nulls that appear must occur for some $t_c > 0$, or more to the point, $\xi(t_c) = \xi_c > 0$. To pinpoint when the solution fails, we must determine when (if at all) the nulls enter the domain $0 < z < L$. This can be done by using the equation $\nabla_\perp\psi = 0$ to derive a relationship between $z_{\rm null}$ (the z coordinate of the nulls) and $\xi(t)$. After some algebra, we obtain

$$z_{\rm null} = \frac{1}{4k}\ln\left(\frac{e^{2kL}\{\cosh\,(2kL) - \cos\,[k\xi(t)]\}}{1 - \cos\,[k\xi(t)]}\right) \quad (36)$$

as the needed formula. Inspection of equation (36) reveals that the initial position of any nulls, i.e., at $\xi|_{t=0} = 0$, occurs only at $z_{\rm null} \to \infty$. This is consistent with the fact that there are no nulls in the initial field inside or outside of the domain. As $\xi(t)$ increases, however, $z_{\rm null}$ decreases monotonically until it finally reaches $z_{\rm null} = L$. Thus the nulls enter the domain of the problem at the top plate, and so it is at this critical displacement, ξ_c, that the solution fails. To summarize, the above solution is valid only for

$$\xi(t) < \xi_c = \frac{1}{k}\arccos\,[e^{-kL}\cosh\,(kL)]\,, \quad (37)$$

and at ξ_c, nulls enter the domain at

$$z_{\rm null} = L\,, \quad x_{\rm null} = \frac{1}{k}\arcsin\,[\pm e^{-kL}\cosh\,(kL)]\,. \quad (38)$$

After $\xi(t_c) = \xi_c$, a new solution must be found. The problem becomes intractable analytically, but can be readily solved numerically. The essential behavior borne out in the simulations is that the emerging null points "stretch out" into y-point discontinuities (Syrovatskii 1971) below the top plate to preserve topology. At these discontinuities are current sheets, with currents in the $\hat{y}$-direction.

The numerical solution is provided by a two-dimensional simulation of the full MHD equations. The code (Guzdar et al. 1993) employs a finite differencing algorithm that is second order in time using trapezoidal leapfrogging and fourth order in space. A small hyperviscosity provides stability. Small viscosity ν and resistivity η are included. The simulation is carried out on a two-dimensional grid; in this case the resolution used is 120 points for each axis, with the domain $0 < z < 1$, $-\pi < x < \pi$. The simulation starts at $t = 0$ with the equilibrium field

$$\psi = e^{-z}\sin\,x\,. \quad (39)$$

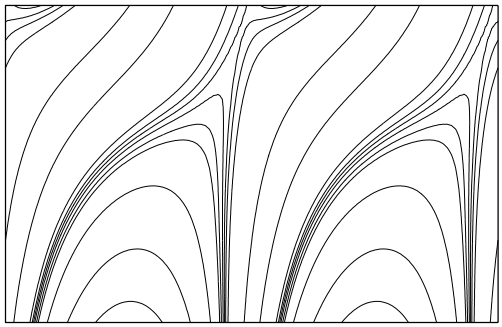

FIG. 2.—Simulation of magnetic field at $\xi = 2.04\xi_c$ in the domain $0 < z < 1$, $-\pi < x < \pi$. Extra contours are plotted near the current sheets for emphasis.

The top boundary is ramped from rest into rigid motion in the x direction according to

$$\xi(t) = \delta(1 - e^{-\delta t}) , \tag{40}$$

where δ is a given parameter. In this case, $\delta = 0.1$ to ensure that the solution remains quasi-static, thus minimizing any Alfvénic effects. Line-tied boundary conditions are used on the z boundaries, while periodic boundary conditions are used on the x boundaries. The simulation is allowed to proceed using a time step $\tau = 0.002$, with η, $\nu = 0.001$ until the critical displacement ξ_c is reached. Current sheets are then observed to form at the two critical points in the domain. Given the relatively small values of ν, η, the current sheets continue to grow without noticeable reconnection for significant $\xi > \xi_c$. Figure 2 shows the current sheets for $\xi = 2.04\xi_c$ (after some noticeable reconnection), and Figure 3 shows a closeup of one of the current sheets. However, the reconnection process, driven by η, eventually smoothes out the current sheets, and the equilibrium solution is regained by the time $\xi = \pi$.

5. DISCUSSION

Starting from a relatively simple magnetic configuration, we have shown that relatively simple motions of footpoints can give rise to current sheets, i.e., step discontinuities in magnetic fields. This result supports a well-investigated but

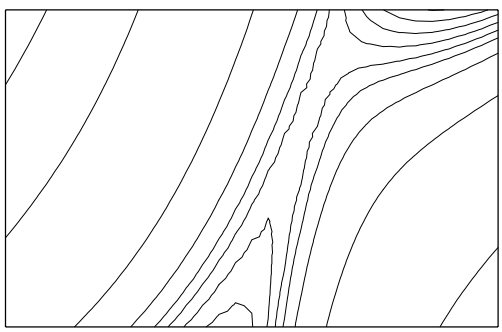

FIG. 3.—Closeup of current sheet at $\xi = 2.04\xi_c$ in the domain $0.76 < z < 1$, $-0.31\pi < x < 0.21\pi$.

contentious theory of Parker that continuous quasi-static deformations of footpoints result in neighboring MHD equilibria that are not generally continuous themselves. The resulting current sheets may heat the corona sufficiently to explain the hot corona. One of the reasons for the contention accompanying this theory is the difficulty in finding analytically simple examples that demonstrate Parker's point. We were motivated to find simple examples of current sheet formation and have been able to present two in this paper. Our model is two-dimensional, thus allowing analytical tractability. Other two-dimensional calculations involving axial displacements (our case 1) (Low 1991; Vekstein et al. 1991) and transverse displacements (our case 2) (Low 1987, 1989; Low & Wolfson 1988) have been reported. As in our cases, these systems feature initial magnetic fields lacking nulls or discontinuities, and they are driven by slow deformations. The examples involving axial displacements possess topologies similar to our case 1. We come to essentially the same conclusion that infinitesimal displacements can lead to current sheets in such cases. Whereas their approaches are more general, we give a simple, specific example. Unlike our case 2, the examples involving transverse displacements use footpoint compressions that are not explicitly given as a function of time. Thus only the end states are calculated without clearly showing the dynamics of the developing current sheets. In any case, the magnetic configurations used are considerably more complicated than those presented here.

For the examples in this paper to be at all applicable to the solar corona, they must in some way correspond to possible three-dimensional configurations. When extending the analogy to three dimensions, the important features of the two-dimensional model should be preserved so that the essential physics remains qualitatively the same. With this in mind, consider the three-dimensional potential field sketched in Figure 4. Loosely speaking, the geometry is that of our two-dimensional model folded over so that both of the boundaries coincide with the photospheric boundary. The footpoints are spaced far enough apart so that their displacements may be considered uncorrelated; in this sense the footpoints on the left are analogous to our bottom plate, while those on the right are analogous to our top plate. Note that the essential characteristics of region I and II field lines are preserved, and accordingly there is still a critical field line that just grazes the right-hand footpoint. Although it is by no means proved, one can imagine how displacements of any of the footpoints might generate current sheets at the critical field line in analogy with the results of the two-dimensional examples. Assuming that current sheets of this nature are possible, the essential physics seems to stem from the diverging nature of neighboring field lines at the discontinuities: the field lines near current sheets may emerge from the photosphere very close together, but reenter the photosphere very far apart, in footpoints that are not causally connected. Thus the independent motions of the footpoints could drive correspondingly independent perturbations of neighboring field lines, causing discontinuities.

An important caveat to the above scenario (Karpen, Antiochos, & DeVore 1990) deserves mention at this point. An important characteristic of the magnetic field in our model is that there are no preexisting nulls. This being the case, region II field lines that are close neighbors of the critical field line presumably do not penetrate very far into

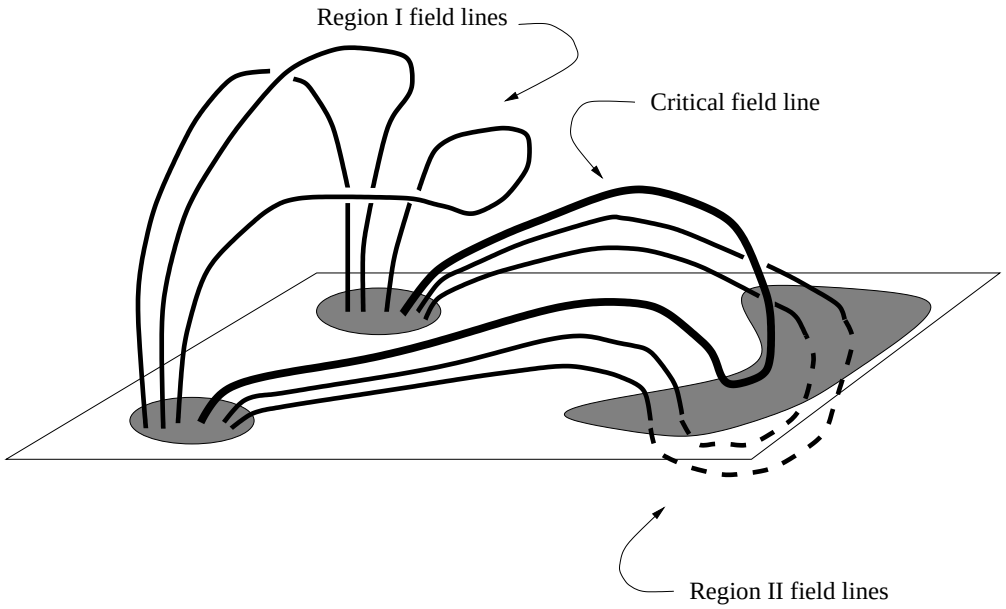

FIG. 4.—Three-dimensional analogy of the two-dimensional model problem. Note that the regions and critical field line correspond qualitatively to Fig. 1.

the photosphere (see the dashed lines of Fig. 4). Thus for field lines that penetrate an arbitrarily short distance into the photosphere, the gravitational scale height of the solar atmosphere needs to be considered. Two-dimensional simulations carried out by Karpen et al. (1990) show that potential discontinuities near the corona-photosphere boundary will be smoothed out over this scale. The physics is straightforward: field lines that do not penetrate substantially into the photosphere cannot be efficiently anchored by the footpoint inertia. Thus footpoint slippage occurs for these field lines. Field line slippage becomes negligible below a depth greater than the gravitational scale height and so over that distance the magnetic field can undergo a continuous transition from region I to region II. It should be noted that the interpretation of the simulations by Karpen et al. (1990) have been debated. Low (1991) points out that the magnetic Reynolds numbers achievable numerically are only about 10^3, obviously incommensurate with the magnetic Reynolds number in the corona that can be as large as 10^{18}: a small Reynolds number could prevent or at least delay the appearance of current sheets. Note, however, that our simulations indeed show the development of current sheets for correspondingly small Reynolds numbers. Another perhaps more physically relevant point is that the gravitational scale height could be small enough to allow relatively thin current systems to develop, thus retaining the qualitative properties of current sheet development.

To conclude, the two-dimensional examples presented here highlight the importance of diverging magnetic fields in the development of spontaneous current sheets. Analogies to the full three-dimensional problem, as discussed above, are as yet unproved, but certainly show promise as potential candidates for three-dimensional discontinuities in previously quasi-static, continuous magnetic fields.

This work was supported in part by the NSF.

REFERENCES

Antiochos, S. K. 1987, ApJ, 312, 895
Guzdar, P. N., Drake, J. F., McCarthy, D., Hassam, A. B., & Liu, C. S. 1993, Phys. Fluids B, 5(10), 3712.
Hassam, A. B., & Lambert, R. P. 1996, ApJ, 472, 832
Karpen, J. T., Antiochos, S. K., & DeVore, C. R. 1990, ApJ, 356, L67
Low, B. C. 1987, ApJ, 323, 358
———. 1989, ApJ, 340, 558
———. 1991, ApJ, 381, 295
Low, B. C., & Wolfson, R. 1988, ApJ, 324, 574
Parker, E. N. 1994, Spontaneous Current Sheets in Magnetic Fields (New York: Oxford Univ. Press)
Syrovatskii, S. I. 1971, Soviet Phys.—JETP. 33, 5, 933
Van Ballegooijen, A. A. 1985, ApJ, 298, 421
Vekstein, G., Priest, E. R., & Amari, T. 1991, A&A, 243, 492.
Zirker, J. B. 1993, Sol. Phys., 148, 43.